Development of Algorithms and Signal Enhancement Techniques for Seismocardiogram-Based Hemodynamic Parameter Estimation

by

Berke Kizir

A Dissertation Submitted to the
Graduate School of Sciences and Engineering
in Partial Fulfillment of the Requirements for
the Degree of

Master of Science

in

Computer Science and Engineering

KOÇ ÜNİVERSİTESİ

January 17, 2025

Development of Algorithms and Signal Enhancement Techniques for Seismocardiogram-Based Hemodynamic Parameter Estimation

Koç University

Graduate School of Sciences and Engineering

This is to certify that I have examined this copy of a master's thesis by

Berke Kizir

and have found that it is complete and satisfactory in all respects,

and that any and all revisions required by the final

examining committee have been made.

Committee Members:

____

Assist. Prof. Beren Semiz Gürsoy (Advisor)

____

Assoc. Prof. Nurcan Tunçbağ

____

Prof. Mehmet Burçin Ünlü

Date: ________________________________

ABSTRACT

Development of Algorithms and Signal Enhancement Techniques for Seismocardiogram-Based Hemodynamic Parameter Estimation

Berke Kizir

Master of Science in Computer Science and Engineering

January 17, 2025

Continuous monitoring plays a critical role in bridging the information gap that exists between periodic hospital visits. Recent advancements in sensor technology and biomedical signal processing have paved the way to the development of sensor systems capable of continuous monitoring of physiological signals and diagnosing various pathologies. Among various types of physiological signals, the seismocardiogram (SCG) is particularly popular in wearable system design. The SCG corresponds to the chest micro-vibrations caused by blood ejection and heart contraction during each cardiac cycle. This thesis focuses on developing algorithms to derive various hemodynamic parameters and enhancement methods for SCG signal analysis. These methods aim to improve signal quality, enable accurate feature extraction, and enhance the reliability of SCG-based physiological assessment. Chapter 2 explores the temporal and spectral relationships between SCG signals and hemodynamic parameters like pre-ejection period (PEP) and left ventricular ejection time (LVET). It presents regression models to estimate these parameters and investigates the relationship between thorax impedance and SCG-derived features. Chapter 3 introduces a two-step hierarchical framework for apnea detection and respiration pace assessment using SCG signals. This model includes binary classification for detecting breath-holding episodes and multi-class classification for categorizing breathing patterns (normal, slow, fast). Chapter 4 presents a comparative evaluation of various denoising algorithms aimed at improving SCG signal quality during exercise. It assesses the performance of different heart rate estimation methods and compares the impact of seven different denoising algorithms on SCG-based heart rate estimation. Overall, these findings collectively support the versatility and potential of SCG in advancing personalized healthcare, particularly in wearable health monitoring and continuous physiological assessment.

ÖZETÇE

Sismokardiyogram Tabanlı Hemodinamik Parametre Tahmini için Algoritma Geliştirme ve Sinyal İyileştirme Teknikleri

Berke Kizir

Bilgisayar Bilimleri ve Mühendisliği, Yüksek Lisans

17 Ocak 2025

Sürekli izleme, periyodik hastane ziyaretleri arasındaki bilgi boşluğunu kapatmada kritik bir rol oynamaktadır. Son dönemdeki sensör teknolojisi ve biyomedikal sinyal işleme alanındaki ilerlemeler, fizyolojik sinyalleri sürekli olarak izleme ve çeşitli patolojileri teşhis etme kapasitesine sahip sensör sistemlerinin geliştirilmesinin önünü açmıştır. Fizyolojik sinyaller arasında, seismokardiyogram (SCG)**,** giyilebilir sistem tasarımında yaygın olarak kullanılmaktadır. SCG, kardiyak döngü sırasında kanın pompalanması ve kalp kasılmasından kaynaklanan göğüs mikro titreşimleri sonucu oluşur. Bu tez, SCG sinyali analizi için çeşitli hemodinamik parametrelerin türetilmesine yönelik algoritmalar ve iyileştirme yöntemleri geliştirmeye odaklanmaktadır. Bu yöntemler, sinyal kalitesini iyileştirmeyi, doğru özellik çıkarımını sağlamayı ve SCG tabanlı fizyolojik değerlendirmelerin güvenilirliğini artırmayı hedeflemektedir. Bölüm 2, SCG sinyalleri ile ön-ejeksiyon süresi (PEP) ve sol ventriküler ejeksiyon süresi (LVET) gibi hemodinamik parametreler arasındaki zamansal ve spektral ilişkileri incelemektedir. Bu parametreleri tahmin etmek için regresyon modelleri sunmakta ve toraks empedansı ile SCG'den türetilen özellikler arasındaki ilişkiyi araştırmaktadır. Bölüm 3, SCG sinyalleri kullanarak uyku apnesi tespiti ve solunum hızı değerlendirmesi için iki aşamalı bir hiyerarşik model sunmaktadır. Bu model, nefes tutma (apne) epizodlarını tespit etmek için ikili sınıflandırma ve solunum desenlerini (normal, yavaş, hızlı) kategorize etmek için çoklu sınıflandırma içermektedir. Bölüm 4, egzersiz sırasında SCG sinyali kalitesini iyileştirmeyi amaçlayan çeşitli gürültü giderme algoritmalarının karşılaştırmalı bir değerlendirmesini sunmaktadır. Bu doğrultuda farklı kalp hızı tahmin yöntemlerinin performansını değerlendirmekte ve yedi farklı gürültü giderme algoritmasının SCG tabanlı kalp hızı tahmini üzerindeki etkisini karşılaştırmaktadır. Genel olarak bu bulgular, SCG'nin kişiselleştirilmiş sağlık hizmetlerini geliştirmedeki çok yönlülüğünü, giyilebilir sağlık izlemede kullanılabilirliğini ve sürekli fizyolojik değerlendirmedeki potansiyelini destekler niteliktedir.

ACKNOWLEDGEMENTS

I would like to express my heartfelt gratitude to my advisor Assist. Prof. Beren Semiz Gürsoy for her continuous and invaluable support throughout my academic journey. Her wisdom, patience and guidance have been instrumental in shaping and completing this thesis.

I also would like to thank Prof. Mehmet Burçin Ünlü and Assoc. Prof. Nurcan Tunçbağ for accepting to be in my thesis jury, reviewing my work and providing invaluable feedback.

I am grateful to TÜBİTAK for their financial support through the 2210-A scholarship program.

Finally, I would like to thank my family for their support and love.

TABLE OF CONTENTS

1. List of Tables ... viii

2. List of Figures ... ix

3. Abbreviations ... x

Chapter 1: Introduction ... 1

1.1 Background and Problem Statement ... 1

1.2 Additional Signals used in the Thesis ... 2

1.3 Contributions of the Thesis ... 3

Chapter 2: Unveiling the Temporal and Spectral Relationships between Seismocardiogram Signals, Systolic Time Intervals and Thorax Characteristics ... 5

2.1 Problem Statement ... 5

2.2 Methods ... 6

2.2.1 Dataset Description ... 6

2.2.2 Pre-processing and Data Preparation ... 7

2.2.3 Feature Extraction ... 8

2.2.4 Model Training and Feature Importance Analysis ... 9

2.2.5 Body Impedance Correlation Analysis ... 10

2.3 Results and Discussion ... 10

2.3.1 PEP and LVET Estimation ... 10

2.3.2 Feature Importance Ranking ... 11

2.3.3 Correlation with Thorax Impedance ... 12

2.4 Conclusion ... 12

Chapter 3: A Hierarchical Framework for Apnea Detection and Respiration Pace Assessment using Seismocardiogram Signals ... 14

3.1 Problem Statement ... 14

3.2 Methods ... 15

3.2.1 Data Collection Protocol ... 15

3.2.2 Pre-processing 16

3.2.3 Feature Extraction.. 17

3.2.4 Model Training and Feature Importance Analysis 19

3.3 Results and Discussion 21

3.3.1 Apnea Detection Results 21

3.3.2 Breathing Rate Assessment 22

3.3.3 Effect of Window Length 22

3.3.4 Feature Importance Ranking 23

3.4 Conclusion 25

Chapter 4: Comparative Evaluation of Denoising Algorithms for Enhanced SCG Signal Processing during Exercise 26

4.1 Problem Statement.. 26

4.2 Methods 27

4.2.1 Custom Wearable Patch.. 27

4.2.2 Experimental Setup and Dataset Information....................................... 27

4.2.3 Preprocessing.. 29

4.2.4 Heart Rate Computation in Resting Phase 29

4.2.5 Heart Rate Computation in Exercise Phase 31

4.2.6 Denoising Algorithms... 31

4.3 Results and Discussion 33

4.3.1 Heart Rate Results for Rest and Exercise Phases 33

4.3.2 Effect of Enveloping.. 33

4.3.3 Effect of Denoising Methods... 35

4.4 Conclusion 35

Chapter 5: Conclusion 36

Bibliography 37

1. LIST OF TABLES

Table 1: PEP Prediction - errors given in milliseconds 11
Table 2: LVET Prediction - errors given in milliseconds 11
Table 3: Impedance Pearson Correlations 13
Table 4: Feature Groups 17
Table 5: Performance Comparison (Binary) 21
Table 6: Performance Comparison (Multi-class) 22
Table 7: LGBM Results for Different Window Lengths (Binary) 23
Table 8: LGBM Results for Different Window Lengths (Multi-class) 23
Table 9: SCG Rest Data Heart Rate Calculation Performance 33
Table 10: SCG Exercise Data Heart Rate Calculation Performance 34

2. LIST OF FIGURES

Figure 1: Signals Used in the Analysis 8
Figure 2: PEP and LVET Feature Importance Ranking 12
Figure 3: The Locations of the Sensors 16
Figure 4: Experimental Protocol 16
Figure 5: Study Pipeline 18
Figure 6: Feature Importance Ranking for the Binary and Multi-class Tasks 24
Figure 7: Sensors Locations 28
Figure 8: Experimental protocol 28
Figure 9: Study Pipeline 29

3. ABBREVIATIONS

AC	Aortic Closing
AO	Aortic Opening
BPF	Band Pass Filter
CEEMD	Complementary Ensemble Empirical Mode Decomposition
DT	Decision Tree
ECG	Electrocardiogram
EEMD	Ensemble Empirical Mode Decomposition
EMD	Empirical Mode Decomposition
FN	False Negatives
FP	False Positives
HR	Heart Rate
ICG	Impedance Cardiography
LGBM	Light Gradient Boosting Machine
LVET	Left Ventricular Ejection Time
MA	Moving Average
MAE	Mean Absolute Error
PEP	Pre-ejection Time
PSG	Polysomnography
RMSE	Root Mean Squared Error
RF	Random Forest
SCG	Seismocardiogram
SG	Savitzky-Golay
STI	Systolic Time Interval
TN	True Negatives
TP	True Positives
XGB	Extreme Gradient Boosting Trees
VMD	Variational Mode Decomposition

CHAPTER 1: **INTRODUCTION**

1.1 Background and Problem Statement

Continuous monitoring plays a critical role in bridging the information gap that exists between periodic hospital visits. Traditional clinical assessments provide only a snapshot of an individual’s health, often missing fluctuations or early signs of deterioration that occur between appointments. By enabling real-time data collection and analysis, continuous monitoring offers a more comprehensive view of a patient’s health status, ultimately improving patient outcomes and reducing the burden on healthcare systems. This approach not only facilitates earlier detection of abnormalities but also supports timely interventions, offers proactive and preventive care strategies, and supports the creation of personalized treatment plans [Sana et al., 2020].

Recent advancements in sensor technology and biomedical signal processing have paved the way to the development of sensor systems capable of continuous monitoring of physiological signals and diagnosing various pathologies. The electrical, mechanical, acoustic, and optical signals recorded from the human body via sensor systems directly result from anatomical mechanisms occurring in the body, providing clinically valuable insights into underlying physiological conditions [Cheol Jeong et al., 2018]. Indeed, analyzing these signals with appropriate algorithms can help in extracting clinically useful parameters and models to complement the conventional clinical practices.

Among various types of physiological signals, the seismocardiogram (SCG) is particularly popular in wearable system design. The SCG corresponds to the chest micro-vibrations caused by blood ejection and heart contraction during each cardiac cycle [Inan et al, 2014]. The diagnostic potential of the SCG signal was first recognized in 1992, when it was found to enhance the effectiveness of the exercise stress test [Salerno et al., 1992]. Later studies demonstrated that combining SCG with ECG signals provided better diagnostic outcomes for coronary artery disease (CAD) compared to using ECG alone [Wilson et al., 1993].

The SCG signal can be measured from any location on the body in three main planes when triaxial accelerometers are used, and the signal in each axis exhibits a unique shape and pattern. These signals are characterized by distinct peaks and valleys, corresponding to specific physiological events such as aortic opening (AO) and aortic closing (AC). SCG frequency components include respiration-related chest movements (<1 Hz), cardiac vibrations (1–20 Hz), and heart sounds (>20 Hz) [Pandia et al., 2012]. Since SCG signals provide a comprehensive view of the thoracic region, they are widely used in wearable systems designed to monitor cardiovascular and cardiopulmonary conditions [Hayirlioglu and Semiz, 2023]. Previous research has indicated that SCG signals can be utilized for detecting heart failure [Inan et al., 2018], aortic stenosis [Yang et al., 2020], and atrial fibrillation [T. Hurnanen et al., 2016], as well as for predicting stroke volume values [Semiz et al., 2020], estimating systolic time intervals [Shandhi et al., 2019], classifying valvular heart disease locations [Erin and Semiz, 2023], and assessing respiration phases [Imirzalioglu and Semiz, 2022, Pandia et al., 2012].

This thesis focuses on developing algorithms to derive various hemodynamic parameters (such as pre-ejection period, left ventricular ejection time, heart rate and breathing patterns) and enhancement methods (particularly pre-processing and denoising) for SCG signal analysis. These methods aim to improve signal quality, enable accurate feature extraction, and enhance the reliability of SCG-based physiological assessments.

1.2 Additional Signals used in the Thesis

Although the main focus was on the SCG analysis, electrocardiogram and impedance cardiography measurements have also been leveraged as reference measurements in different tasks throughout the thesis. Below, short background information about both signals is presented:

<u>Electrocardiogram (ECG):</u> ECG provides information about the electrical activity of the heart and is recorded using electrodes attached to the surface of the body. It consists of three main components: the P wave, the QRS complex, and the T wave. The P wave results from the depolarization of the atria, the QRS complex from the depolarization of the ventricles, and the T wave from the repolarization of the ventricles [Odinaka et al.,

2012]. Each segment between two consecutive R peaks in an ECG signal corresponds to a single heartbeat and typically varies between 600-1000 ms. After calculating the average R-R interval length, the average heart rate can easily be determined. The analysis of ECG signals plays a role in assessing various heart conditions, including coronary artery disease, arrhythmias, and cardiomyopathy.

Impedance Cardiography (ICG): ICG measures changes in electrical impedance throughout the cardiac cycle. Since electrical signals naturally follow paths of least resistance, they primarily travel through the fluid-filled aorta, as blood is more conductive than surrounding tissues [Summers et al., 2003]. To measure ICG, mostly the 8-electrode configuration is used. The 8-electrode configuration involves placing four pairs of electrodes on the body: two on the neck and two on the thorax near the lower rib cage. The other electrodes inject a small, high-frequency electrical current, whereas the inner electrodes measure the changes in voltage due to impedance variations caused by blood flow and cardiac activity. Variations in impedance can be linked to several hemodynamic parameters. The interval between the B and X points on the ICG signal is used to calculate left ventricular ejection time (LVET), while pre-ejection period (PEP) is defined as the time between the Q-peak of the ECG signal and the B point on the ICG [Sherwood et al., 1990].

1.3 Contributions of the Thesis

This thesis primarily focuses on developing algorithms to derive various hemodynamic parameters from SCG signals, as well as evaluating different SCG denoising pipelines to address motion-related noise. Chapter-wise contributions of this thesis can be listed as follows:

- *Chapter 2: Unveiling the Temporal and Spectral Relationships Between Seismocardiogram Signals, Systolic Time Intervals and Thorax Characteristics*
    - Developing SCG-based PEP and LVET regression models utilizing both temporal and spectral analyses,
    - Identifying the most distinctive features for systolic time interval (STI) estimation beyond AO and AC points,

    - Exploring the relationship between thorax impedance values and SCG-derived features to quantify inter-subject variability.
- *Chapter 3: A Hierarchical Framework for Apnea Detection and Respiration Pace Assessment using Seismocardiogram Signals*
    - Developing a novel two-step hierarchical framework for apnea detection and respiration pace assessment using SCG signals: (i) a binary classification model to detect breath-holding (apnea) episodes, and (ii) a multi-class classification model to distinguish between normal, slow, and fast breathing episodes,
    - Investigating the optimal window length for real-time apnea detection and breathing rate assessment.
- *Chapter 4: Comparative Evaluation of Denoising Algorithms for Enhanced SCG Signal Processing during Exercise*
    - Assessing the performance of four different SCG-based heart rate estimation methods during resting and exercise phases: (i) directly implementing peak finding, (ii) enveloping and peak finding, (iii) applying Teager-Kaiser operator and peak finding, and (iv) applying Teager-Kaiser operator, enveloping and peak finding,
    - Evaluating and comparing the improvement in the SCG-based heart rate estimation results under seven different denoising algorithms: empirical mode decomposition (EMD), Ensemble EMD (EEMD), Complementary Ensemble EMD (CEEMD), Variational Mode Decomposition (VMD), Savitzky-Golay filtering, moving average employement and wavelet denoising.

CHAPTER 2: UNVEILING THE TEMPORAL AND SPECTRAL RELATIONSHIPS BETWEEN SEISMOCARDIOGRAM SIGNALS, SYSTOLIC TIME INTERVALS AND THORAX CHARACTERISTICS

2.1 Problem Statement

The cardiac cycle is composed of four key phases: isovolumetric relaxation, diastolic filling, isovolumetric contraction, and systolic ejection [Lewis et al., 1977]. Examining the duration of these phases provides valuable information about cardiovascular health and the functioning of the autonomic nervous system. Notably, systolic time intervals (STIs) have been shown to correlate with factors such as preload, ventricular pressure dynamics, ventricular failure, and other important indicators [Tavakolian, 2016]. Among these STIs, the left ventricular ejection time (LVET) and the pre-ejection period (PEP) are particularly significant. PEP refers to the time interval from ventricular excitation to the opening of the aortic valve, while LVET measures the duration of blood ejection from the ventricles [Javaid et al., 2015]. Although echocardiography allows for the assessment of STIs, it is limited to clinical settings, highlighting the need for innovative technologies capable of continuously monitoring cardiovascular parameters in everyday environments.

Recent research has demonstrated that both electrical and mechanical evaluations of the cardiovascular system can offer critical insights into underlying health conditions. The electrocardiogram (ECG) reflects the electrical activity of the heart, originating from the heart muscle's polarization cycle, while the seismocardiogram (SCG) provides a mechanical perspective by capturing local chest vibrations caused by blood ejection [Inan et al, 2014]. Studies have shown that PEP and LVET can be estimated from SCG signals using the aortic opening (AO) and aortic closing (AC) points as reference markers [Javaid et al., 2015, Shandhi et al., 2019, Di Rienzo et al., 2013]. Specifically, LVET is defined as the time interval between the AO and AC points on the SCG, while PEP represents the duration from the R-peak of the ECG to the AO point on the SCG. However, due to the susceptibility of SCG signals to motion artifacts [Lin et al., 2021], accurately detecting AO and AC points remains challenging, making AO- and AC-based STI analysis less reliable and difficult to generalize.

On the other hand, impedance cardiography (ICG) measures changes in electrical impedance throughout the cardiac cycle. As previously explained, the interval between the B and X points on the ICG signal is used to calculate LVET, while PEP is defined as the time between the Q-peak of the ECG signal and the B point on the ICG [Sherwood et al., 1990]. A recent study proposed an SCG-based PEP regression model, using ICG-derived PEP values as reference [Shandhi et al., 2019]. However, two significant challenges remain: (i) reliably estimating LVET from SCG signals using regression analysis and (ii) understanding the impact of thorax characteristics on STI estimation.

The contributions of this study are as follows: to the best of our knowledge, this is the first work to (i) develop SCG-based PEP and LVET regression models utilizing both temporal and spectral analyses, (ii) identify the most distinctive features for STI estimation beyond AO and AC points, and (iii) explore the relationship between thorax impedance values and SCG-derived features to quantify inter-subject variability. These findings offer valuable insights into SCG and thorax characteristics, paving the way for more effective and informative SCG-based STI analysis.

2.2 Methods

2.2.1 Dataset Description

This study was approved by the Koc University Institutional Review Board, and all participants provided written informed consent. A total of 14 healthy individuals (7 males and 7 females; height: 171.8 ± 8.2 cm; weight: 68.2 ± 14.9 kg; age: 23.1 ± 2.6 years) participated in the study. On the morning of data collection, body composition was analyzed using the Tanita BC-418 Segmental Body Composition Analyzer (Tanita Corporation of America, Inc., IL, USA). Following this, physiological signals were collected.

All signals were recorded using the BIOPAC system (BIOPAC Systems, Inc., Goleta, CA, USA). ECG signals were captured using three gel electrodes, while respiration data was acquired via a respiratory effort transducer belt. For the impedance ICG signal, eight gel electrodes (four for current and four for voltage) were positioned around the neck and below the chest. The respiration, ECG, and ICG signals were wirelessly transmitted to the BIOPAC system using the Bionomadix RSPEC-R and NICO modules. Additionally, an SCG signal was collected using a low-noise tri-axial analog accelerometer (ADXL354, Analog Devices, Inc., Norwood, MA) placed on the mid-sternum. The accelerometer captured signals along the X (lateral), Y (head-to-foot), and Z (dorso-ventral) axes. All signals were recorded concurrently at a sampling rate of 2 kHz.

The data collection protocol involved continuous recording. Initially, the subject stood upright for three minutes in a resting condition. This was followed by a 20-second breath-holding period (Valsalva maneuver) and a subsequent two-minute rest period. To further induce physiological changes, the subject performed a stepping exercise for one minute at a pace of 90 beats per minute, followed by a one-minute squatting exercise. While these exercises elevated heart rate, they also reduced the durations of PEP and LVET. At the end of the exercise session, the subject returned to a stationary standing position and remained at rest for five minutes. For the analysis, three minutes of data from the initial rest period and the last four minutes of the final recovery period were used. Data from the recovery phases between physiological modulation steps, as well as the first minute of the last recovery period, were excluded. Additionally, one subject's data was excluded due to poor quality caused by hardware-related issues, leaving 13 subjects for the analysis.

2.2.2 Pre-processing and Data Preparation

The signals were first filtered using a Kaiser window finite impulse response filter to remove out-of-band noise. The cut-off frequencies were set to 1-40 Hz for SCG, 0.5-40 Hz for ECG, and 1-30 Hz for ICG. After filtering, a Gaussian window was applied to smooth micro-oscillations in the signals, with a window length of 50 for SCG and 200 for both ECG and ICG. Following pre-processing, the R and Q points were detected on the ECG signal. The R-R intervals were calculated based on the consecutive R-peak locations, representing the corresponding beat lengths. Using these R-R intervals, the SCG and ICG signals were divided into individual beats. Notably, any R-R interval exceeding 1.5 seconds was excluded during this segmentation process. Sample beats from each signal are shown in Figure 1.

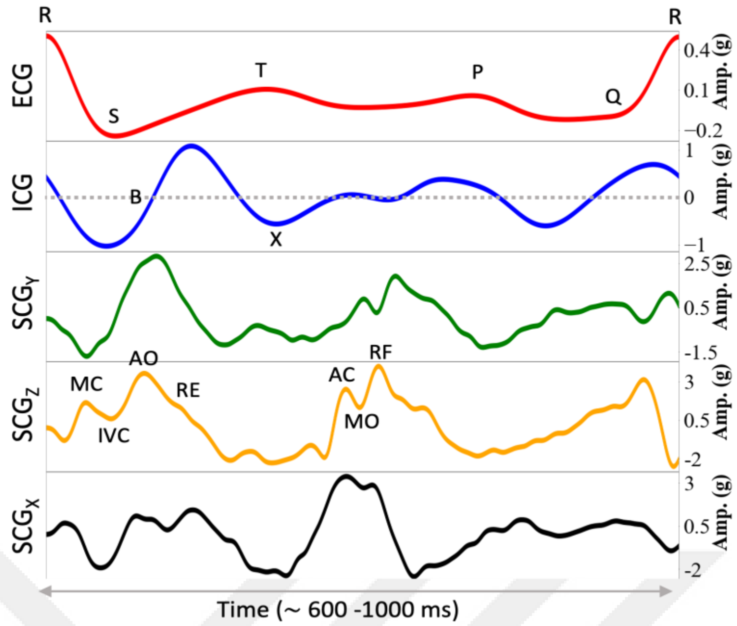

Figure 1: Signals Used in the Analysis

For each ICG beat, the B and X points were identified to compute the reference PEP and LVET values. The B point serves as the reference for the aortic valve opening and marks the start of ventricular ejection [Shandhi et al., 2019]. On any given ICG beat, the B point was located at the upward zero-crossing of the signal. The PEP value was then determined by calculating the time difference between the Q point at the onset of the corresponding ECG beat and the B point on the same ICG beat. Similarly, the X point represents the reference for aortic valve closing. For each ICG beat, the X point was identified as the lowest point (minimum) within the segment from the B point to the end of the beat. The LVET value was calculated as the time interval between the B and X points.

In the final step, a quantile filter was applied to minimize the impact of inaccurately detected reference points. Specifically, PEP and LVET values below the 10th percentile and above the 90th percentile were excluded. After removing outliers and low-quality beats, a total of 4,214 beats remained for analysis.

2.2.3 Feature Extraction

Previous studies have demonstrated that SCG analysis can significantly benefit from both temporal and spectral analyses [Erin and Semiz, 2023, Semiz et al., 2020]. Consequently, statistical, time-domain, and frequency-domain features were extracted from each SCG beat.

For statistical features, mean, variance, skewness, and kurtosis were calculated. In the time-domain analysis, the beat energy was computed first. The remaining analysis was divided into two parts: the first half (first 250 ms) and the second half (remaining portion of the beat). In the first half, the locations and widths of the first and second peaks, as well as the first and second minima, were measured. For the second half, only the locations and widths of the first peak and the first minimum were considered.

In the frequency-domain analysis, spectral centroid, spectral spread, and spectral rolloff were extracted. Additionally, the bandpowers of 14 logarithmically spaced frequency bands between 25 and 1000 Hz were calculated.

For the regression analysis, four different training configurations were implemented: (i) using features from only the x-axis, (ii) using features from only the y-axis, (iii) using features from only the z-axis, and (iv) using features from all three axes combined.

2.2.4 Model Training and Feature Importance Analysis

2.2.4.1 Model Selection and Performance Assessment

Extreme Gradient Boosting (XGB) was selected as the regression model [Chen and Guestrin, 2016]. For each PEP and LVET estimation task, four separate regression models were trained as previously outlined. A 5-fold cross-validation approach was employed for all tasks. Model performance was evaluated using four metrics: root mean squared error (RMSE), mean absolute error (MAE), mean absolute percentage error (MAPE), and correlation (R).

2.2.4.2 Feature Importance Ranking

For both PEP and LVET regression tasks, XGB-based feature importance ranking was utilized to identify the most critical features for the estimation. Within each fold of the XGB framework, feature rankings and their corresponding importance scores were computed. After completing all folds, the average score for each feature was calculated to generate the overall importance ranking.

2.2.5 Body Impedance Correlation Analysis

A significant challenge in the analysis of physiological signals is inter-subject variability, which arises from differences in physiology, anatomy, and responses to stressors among individuals. This variability makes it difficult for machine learning models to consistently learn clinically relevant patterns in the signals, often leading to increased errors. While subject-specific models have been proposed as a solution, this approach restricts the generalizability of the frameworks, limiting their applicability to broader populations [Xu et al., 2014].

The path from the heart to the accelerometer traverses multiple layers, including bone, muscle, fat, and skin tissues, which influence the thorax medium and its impedance. Understanding the relationship between thorax impedance and SCG signal characteristics may offer valuable insights into the contribution of inter-subject variability to measurement errors. A previous study investigated the effect of inter-subject variability on SCG and ICG signals [Shandhi et al., 2019].

In this study, inter-subject variability in SCG signals was further assessed by analyzing the correlation between thorax impedance and SCG features. Since each subject had only one thorax impedance value obtained from the Tanita Analyzer, the mean of each SCG feature was first calculated. Pearson correlation analysis was then conducted to evaluate the relationships.

2.3 Results and Discussion

2.3.1 PEP and LVET Estimation

For PEP estimation, when features from all axes were combined, the model achieved an R value of 0.913, RMSE of 7.436, and MAE of 5.158, along with a notably low MAPE of 3% (Table 1). When evaluating features from individual axes, the Z axis performed the best, followed by the Y axis. This result aligns with expectations since the Z axis reflects contraction strength and the Y axis represents the ejection direction.

Table 1: PEP Prediction - errors given in milliseconds

Metric	All Features	X Features	Y Features	Z Features
R	0.913 ± 0.008	0.833 ± 0.012	0.869 ± 0.009	0.879 ± 0.009
RMSE	7.436 ± 0.341	10.107 ± 0.341	9.043 ± 0.347	8.753 ± 0.272
MAE	5.158 ± 0.142	7.318 ± 0.24	6.422 ± 0.165	6.044 ± 0.161
MAPE	0.03 ± 0.001	0.042 ± 0.001	0.037 ± 0.001	0.035 ± 0.001

Table 2: LVET Prediction - errors given in milliseconds

Metric	All Features	X Features	Y Features	Z Features
R	0.636 ± 0.021	0.57 ± 0.031	0.595 ± 0.029	0.618 ± 0.028
RMSE	11.022 ± 0.34	11.733 ± 0.391	11.478 ± 0.413	11.227 ± 0.429
MAE	7.849 ± 0.321	8.486 ± 0.295	8.218 ± 0.333	8.014 ± 0.333
MAPE	0.063 ± 0.003	0.068 ± 0.002	0.066 ± 0.002	0.064 ± 0.003

For LVET estimation, the model achieved a MAPE of 6.3%, but the R, RMSE, and MAE values were relatively worse at 0.636, 11.022, and 7.849, respectively. Similar to PEP models, LVET models using individual axes followed the same performance trend, with the Z axis outperforming the Y and X axes (Table 2).

2.3.2 Feature Importance Ranking

The top ten most important features for estimating PEP and LVET are illustrated in Figure 2. For PEP estimation, the most critical features included time-domain, statistical, and bandpower features, while no spectral features appeared in the top-ranking list. Among the bandpower features, those corresponding to frequencies above 20 Hz—representing heart sounds—were prominent. For LVET estimation, spectral features were dominant, followed by bandpowers above 590 Hz. Since frequencies between 100 and 1000 Hz are associated with lung sounds, this observation warrants further investigation [Padilla-Ortiz and Ibarra, 2018].

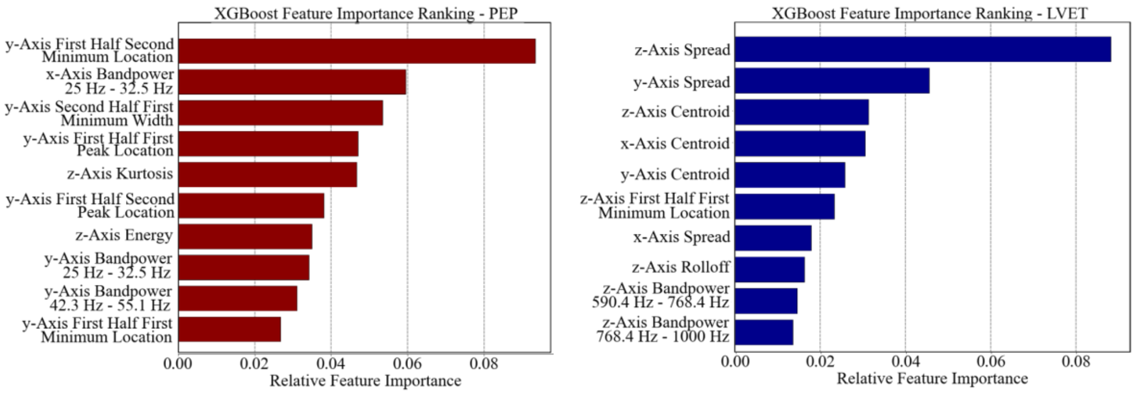

Figure 2: PEP and LVET Feature Importance Ranking

2.3.3 Correlation with Thorax Impedance

The top ten most highly correlated features are presented in Table 3. The bandpower features from the y-axis (71.7 Hz - 93.3 Hz), x-axis (42.3 Hz - 55.1 Hz), and the second minimum width of the first half of z-axis beats exhibited strong negative correlations with thorax impedance. The remaining features showed moderate negative correlations. Additionally, time-domain and bandpower features from all axes were correlated with thorax impedance, with the corresponding bands all having frequencies above 20 Hz, which are associated with the acoustical component (heart sounds) of the SCG signal. These findings suggest that the impedance characteristics of the thorax significantly impact the acoustic properties of the cardiac system.

2.4 Conclusion

In this study, SCG-based PEP and LVET estimation models were developed, utilizing both temporal and spectral analysis. The most important SCG features for PEP and LVET estimation were identified. Additionally, the relationship between SCG signals and thorax impedance values was explored to quantify inter-subject variability. The results showed that PEP and LVET could be estimated with very low RMSE values (7.436 ms and 11.022 ms, respectively). Furthermore, it was found that thorax impedance characteristics are highly correlated with SCG features. Future work will focus on validating these models using larger datasets to improve generalization and incorporating noise reduction algorithms into the framework.

Table 3: Impedance Pearson Correlations

Features (Mean)	**Correlation**
y-Axis Bandpower 71.7 Hz – 93.3 Hz	-0.644
x-Axis Bandpower 42.3 Hz – 55.1 Hz	-0.644
z-Axis First Half Second Minimum Width	-0.621
y-Axis Bandpower 93.3 Hz – 121.5 Hz	-0.599
x-Axis Bandpower 71.7 Hz – 93.3 Hz	-0.578
y-Axis Bandpower 42.3 Hz – 55.1 Hz	-0.568
x-Axis Bandpower 93.3 Hz – 121.5 Hz	-0.558
y-Axis First Half Second Minimum Width	-0.546
y-Axis Bandpower 55.1 Hz – 71.7 Hz	-0.531
x-Axis Bandpower 55.1 Hz – 71.7 Hz	-0.521

CHAPTER 3: A HIERARCHICAL FRAMEWORK FOR APNEA DETECTION AND RESPIRATION PACE ASSESSMENT USING SEISMOCARDIOGRAM SIGNALS

3.1 Problem Statement

Sleep makes up one-third of human life and is essential for physical repair, mental functioning, and memory consolidation [Kwon et al., 2021]. Recent surveys have revealed that 44% of adults have experienced a decline in sleep quality over the past five years, and eight out of ten adults expressed a desire to improve their sleep quality [Philips 2019]. Common sleep disorders include insomnia, sleep apnea, and narcolepsy. Additionally, decreased sleep efficiency due to these issues is linked to secondary conditions such as depression, obesity, diabetes, heart disease, and neurocognitive disorders [Altevogt and Cohen, 2006].

Traditionally, polysomnography (PSG) has been the standard for assessing sleep performance. However, this method requires participants to visit a sleep clinic and have multiple sensors attached to their bodies. While PSG offers a comprehensive evaluation of sleep quality and related issues, monitoring sleep in natural settings (such as at home and without multiple sensors) could provide a more accurate representation of a person's sleep. On the other hand, watch-like devices (such as the Apple Watch) offer sleep monitoring and staging, but these systems rely on customized algorithms based on movement and heart rate. They do not provide detailed information on other vital parameters, such as respiration rate. Therefore, there is a need for alternative methods that enable sleep monitoring outside of clinical settings while maintaining clinical standards.

Recent studies have demonstrated that the seismocardiogram (SCG) signal, collected from the thoracic region, can provide valuable information about various hemodynamic parameters [Inan et al, 2014]. As previously explained, the SCG signal corresponds to the chest micro-vibrations caused by blood ejection and heart contraction during each cardiac cycle. The frequency components of the SCG are as follows: below 1 Hz corresponds to chest movements associated with respiration, 1-20 Hz encompasses cardiac vibrations, and frequencies above 20 Hz are linked to heart sounds [Pandia et al., 2012]. Since SCG signals provide a comprehensive view of the thoracic region, they are widely used in wearable systems designed to monitor cardiovascular and cardiopulmonary conditions [Hayirlioglu and Semiz, 2023].

In this study, we developed a novel hierarchical framework to utilize seismocardiogram (SCG) signals for apnea detection and respiration pace assessment. The framework was tested using a simulated data collection protocol that included breath-holding, slow-breathing, normal-breathing, and fast-breathing episodes. Rather than focusing on the component below 1 Hz, we used the vibration and acoustic components of the SCG signal (1-40 Hz), as apnea types do not necessarily correlate with halted chest movements. In the first step of the framework, a binary classification model was trained to detect breath-holding (apnea) episodes. If the model did not predict a breath-holding state, the data was fed into a second model, a multi-class classification system, designed to differentiate between normal, slow, and fast breathing episodes. Additionally, the optimum window length for real-time apnea detection and breathing rate assessment was investigated. The results demonstrate that SCG signals contain significant information about changes in breathing patterns and could potentially serve as a viable alternative to polysomnography (PSG) for the design of wearable systems.

3.2 Methods

3.2.1 Data Collection Protocol

This study was approved by the Koc University Institutional Review Board, and written consent was obtained from all participants. A total of 8 healthy subjects (6 females and 2 males) took part in the study, with an average age of 21.9 ± 3.0 years, height of 171.6 ± 7.7 cm, and weight of 65.4 ± 12.2 kg. Physiological signals were simultaneously recorded using the BIOPAC system (BIOPAC Systems, Inc., Goleta, CA, USA) at a sampling rate of 2 kHz. The electrocardiogram (ECG) and respiration signals were acquired using three gel electrodes and a respiration transducer, respectively, and transferred to the BIOPAC system via the wireless Bionomadix RSPEC-R module. For seismocardiogram (SCG) signal collection, a tri-axial low-noise analog accelerometer (ADXL354, Analog Devices, Inc., Norwood, MA) was used. The accelerometer was attached to the mid-sternum of each subject using hypoallergenic transparent medical tape. The sensor placement is

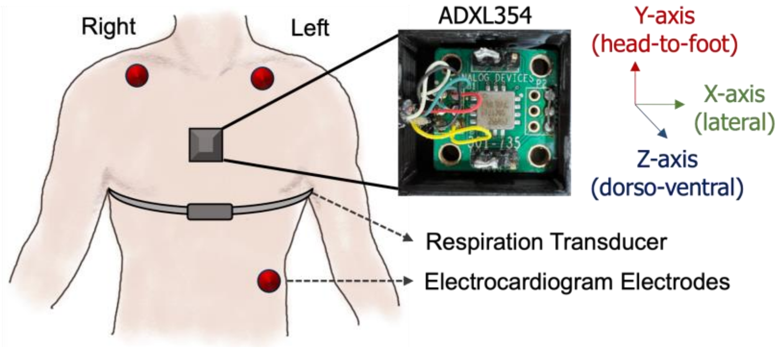

Figure 3: The Locations of the Sensors

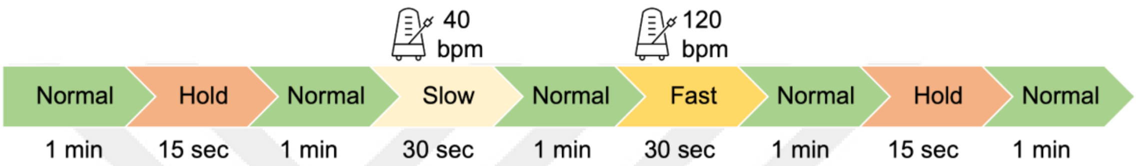

Figure 4: Experimental Protocol

shown in Figure 3. The accelerometer's X, Y, and Z axes correspond to vibrations in the lateral, head-to-foot, and dorso-ventral directions, respectively.

The data collection protocol is detailed in Figure 4. The subject first performed normal breathing for 1 minute, followed by a Valsalva maneuver, where the subject held their breath for 15 seconds. Afterward, the subject returned to normal breathing for another 1 minute. The subject then engaged in slow breathing at a rate of 40 beats per minute (bpm), controlled by an online metronome. Following 1 minute of normal breathing, the subject performed fast breathing at 120 bpm, again controlled by the metronome. The protocol concluded with another 1 minute of normal breathing, followed by a 15-second Valsalva maneuver, and a final 1 minute of normal breathing. Signals were recorded continuously throughout the protocol, with careful timestamps recorded for each transition between the breathing conditions.

3.2.2 Pre-processing

The SCG signals were filtered using a Kaiser window finite impulse response (FIR) filter to remove out-of-band noise. The cut-off frequencies for all three axes were set between 1 and 40 Hz to focus on the relevant frequency components corresponding to cardiac and

Table 4: Feature Groups

Statistical Features	Temporal Features	Spectral Features
Mean	Signal Energy	Centroid
Variance		Spread
Skewness		Rolloff
Kurtosis		Bandpowers (logarithmically spaced between 1 - 40 Hz)

respiratory vibrations. No additional preprocessing steps were applied to preserve all information, including spikes and oscillations, that could be crucial for distinguishing between different breathing states. This approach ensures that the signal retains its full potential for detecting subtle changes in breathing patterns during the experimental protocol.

In this work, one of the primary goals was to evaluate the impact of window length on the performance of apnea detection and respiration rate assessment. To achieve this, the analysis pipeline was repeated using different window lengths (1, 2, 3, 4, and 5 seconds). A 500 millisecond (0.5 seconds) overlap was applied between consecutive windows to increase the number of training instances and enable updates to the subject's breathing state every 0.5 seconds. This approach allows for continuous data streaming, which is essential for real-time apnea detection. Notably, the electrocardiogram (ECG) signal was not used as a reference in this analysis, as the aim was to simulate a real-time scenario where apnea detection could be performed using only SCG signals in a wearable system without the need for additional sensors.

3.2.3 Feature Extraction

Statistical, temporal, and spectral features were extracted from each SCG window across all three axes for analysis (Table 4). The statistical features included mean, variance, skewness (asymmetry), and kurtosis (tailedness), which help quantify the central

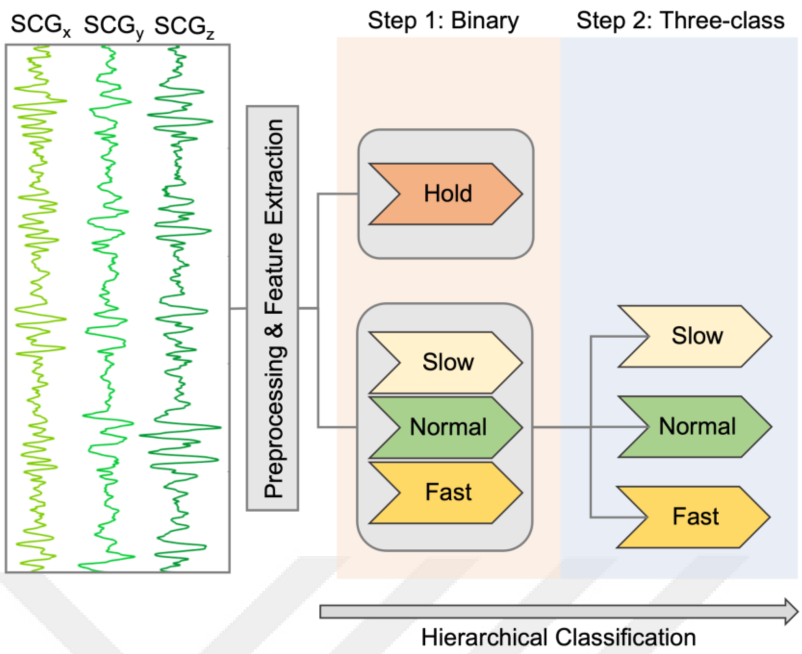

Figure 5: Study Pipeline

tendency and the distribution shape of the SCG signal. The temporal feature calculated was signal energy, which is the squared sum of all the sample values in a given window. This provides information about the magnitude of the signal within each window. In the spectral domain, following features were computed:

- Spectral Centroid: This represents the center of mass of the spectrum and gives an indication of the "brightness" of the signal.
- Spectral Spread: This measures the width of the spectrum, indicating how spread out the frequency components are.
- Spectral Rolloff: The frequency at which a certain percentage of the total signal energy is contained, indicating the cutoff frequency for high-frequency content.
- Bandpower: The power in specific frequency intervals, with logarithmically spaced bands between 1 and 40 Hz, capturing the relevant components of the SCG signal.

Once all features were extracted, a dataframe was generated where each column represented a feature, and each row corresponded to a particular SCG frame. This process was repeated for the different window lengths, ensuring that the analysis accounted for varying time scales. This systematic approach allowed for the comparison of performance across different window lengths, helping to determine the optimal window size for real-time apnea detection and respiration rate assessment.

3.2.4 Model Training and Feature Importance Analysis

3.2.4.1 Hierarchical Model Framework

In this study, a hierarchical model framework was designed to efficiently detect and classify breathing states (Figure 5). The primary focus was to detect breath-holding (apnea) states accurately and quickly, as they are the most critical aspect of the study.

- *Binary Classification Model:* The first model was a binary classifier that distinguished between breath-holding (apnea) and all other states (normal, slow, and fast breathing). In this model, breath-holding (apnea) states were labeled as 1; and normal, slow, and fast breathing were labeled as 0. This classifier's task was to quickly identify breath-holding episodes, ensuring that any periods of apnea could be detected with minimal delay.

- *Multi-Class Classification Model:* If the binary classifier did not predict a breath-holding state (i.e., it predicted a normal, slow, or fast breathing state), the data was passed to the second model, which was a multi-class classification model. The goal of this secondary model was to distinguish between the following types of breathing: Normal breathing, slow breathing (40 beats-per-minute), and fast breathing (120 beats-per-minute).

By using this hierarchical approach, the framework could first and foremost focus on detecting apnea (breath-holding states) as quickly as possible. If the data did not belong to an apnea state, the model then proceeded to classify the type of breathing pattern, ensuring that the system could adapt to any changes in breathing pace between apnea episodes. This structure ensured that the system could handle real-time data streaming, accurately identifying apnea periods and classifying breathing patterns without unnecessary delays.

3.2.4.2 Model Selection and Validation

In this study, four different tree-based models were trained and compared: decision tree (DT), random forest (RF), extreme gradient boosting trees (XGB), and light gradient-boosting machine (LGBM). Given the well-known superior performance of tree-based methods in SCG-related applications, these models were selected. For all classification models, 5-fold cross-validation was applied.

- *Decision Tree (DT):* A decision tree is a flowchart-like structure that uses a divide-and-conquer approach, employing a greedy search to determine the best split points. This process is carried out top-down until the data is assigned class labels [Song and Ying, 2015].
- *Random Forest (RF):* Unlike a single decision tree, random forest (RF) builds multiple trees through bootstrapping, utilizing random subsets drawn from the dataset. These trees are trained independently and in parallel, with majority voting applied to combine their outputs into a final class prediction [Breiman, 2001].
- *Extreme Gradient Boosting Trees (XGB):* XGB is a popular boosting algorithm. Unlike RF, which relies on bagging, XGB works sequentially, where each tree is influenced by the output of the previous one. During training, multiple decision trees are iteratively trained, and the residual errors from earlier iterations are corrected as the training progresses [Chen and Guestrin, 2016].
- *Light Gradient-Boosting Machine (LGBM):* LGBM is another boosting algorithm, but it differs from XGB in that it follows a leaf-wise growth strategy, rather than a level-wise one. This method leads to greater loss reduction, which enhances accuracy and speeds up processing [Ke at al., 2017].

To evaluate the performance of the models, the following metrics were used: accuracy, weighted precision, recall, and F1-score. The equations for these metrics are provided in Equations 1-4, respectively *(TP: true positives, FP: false positives, TN: true negatives, FN: false negatives)*. Additionally, the area under the receiver operating characteristics curve (ROC AUC) was calculated for the binary classification task.

$$Accuracy = \frac{TP + TN}{TP + TN + FP + FN} \qquad (1)$$

Table 5: Performance Comparison (Binary)

Model	Accuracy	AUC	Recall	Precision	F1
LGBM	0.99	0.99	0.95	0.87	0.91
RF	0.94	0.95	0.95	0.30	0.46
XGB	0.99	0.99	0.95	0.85	0.90
DT	0.92	0.73	0.56	0.49	0.52

$$Precision = \frac{TP}{TP + FP} \qquad (2)$$

$$Recall = \frac{TP}{TP + FN} \qquad (3)$$

$$f1\_score = 2 * \frac{precision * recall}{precision + recall} \qquad (4)$$

3.2.4.3 Feature Importance Ranking

Feature importance scores were calculated using the best performing model (LGBM) to identify the most significant features. This process was repeated for both the binary and multi-class classification tasks. After completing all folds, the average of the normalized LGBM scores was computed and considered the final importance score. The scores were then ranked in descending order to establish the feature importance ranking.

3.3 Results and Discussion

3.3.1 Apnea Detection Results

The first step of the hierarchical classification framework involved distinguishing between breath-holding episodes and breathing (normal, fast, slow) periods. For this purpose, a binary classification model was trained. The results obtained from different models using a 5-second window are presented in Table 5. Overall, LGBM and XGB outperformed DT and RF across all metrics. Specifically, precision values from RF and DT were significantly lower than those from the other models, which led to lower f1-

Table 6: Performance Comparison (Multi-class)

Model	Accuracy	Recall	Precision	F1
LGBM	0.96	0.96	0.96	0.96
RF	0.88	0.88	0.94	0.90
XGB	0.95	0.95	0.96	0.96
DT	0.85	0.85	0.85	0.85

scores. While XGB and LGBM performed similarly, LGBM slightly outperformed XGB in terms of precision and f1-score. The accuracy of 0.99 indicated that almost no error was carried over from the binary model to the multi-class task.

3.3.2 Breathing Rate Assessment

Using the primary model, the SCG windows were labeled as breath-holding or not. If the prediction was not breath-holding, the data was passed to a second model, which was designed as a multi-class classification model. The goal of this secondary model was to distinguish between normal, slow, and fast breathing episodes. The performance of the different models is presented in Table 6. As with the binary classification, LGBM and XGB outperformed RF and DT in all metrics. However, the precision and f1-score obtained from RF and DT in the multi-class task were significantly higher than those in the binary task. Overall, LGBM slightly outperformed XGB, similar to the binary task.

3.3.3 Effect of Window Length

As previously mentioned, the ECG was not used as the reference because the real-time apnea detection scenario requires continuous data streaming, which can be achieved through a sliding window. However, determining the optimal analysis window size is a critical research question. Therefore, different window lengths (1, 2, 3, 4, and 5 seconds) were tested to identify the optimal length for the current application. For all experiments, the model used was LGBM.

Table 7: LGBM Results for Different Window Lengths (Binary)

Window Length (sec.)	Accuracy	AUC	Recall	Precision	F1-Score
1	0.95	0.91	0.72	0.51	0.59
2	0.97	0.96	0.86	0.71	0.78
3	0.98	0.97	0.91	0.77	0.83
4	0.98	0.99	0.93	0.83	0.87
5	0.99	0.99	0.95	0.87	0.91

Table 8: LGBM Results for Different Window Lengths (Multi-class)

Window Length (sec.)	Accuracy	Recall	Precision	F1-Score
1	0.85	0.85	0.88	0.86
2	0.90	0.90	0.92	0.91
3	0.93	0.93	0.94	0.93
4	0.95	0.95	0.96	0.95
5	0.96	0.96	0.96	0.96

The performance values for the binary and multi-class tasks with varying window lengths are presented in Tables 7 and 8. When the window length was set to 1 second, the results significantly worsened for both tasks. In the binary case, the recall value dropped to 0.72 with 1-second windows, representing a 24% decrease compared to the performance with 5-second windows. Window lengths longer than 5 seconds produced similar results, and when the window length exceeded 10 seconds, performance began to decline. A similar pattern was observed for the multi-class task. Based on these observations, the optimal window length was determined to be 5 seconds.

3.3.4 Feature Importance Ranking

Feature importance scores were computed from the LGBM classifier, and after all folds were completed, the average of the normalized scores was calculated as the final score.

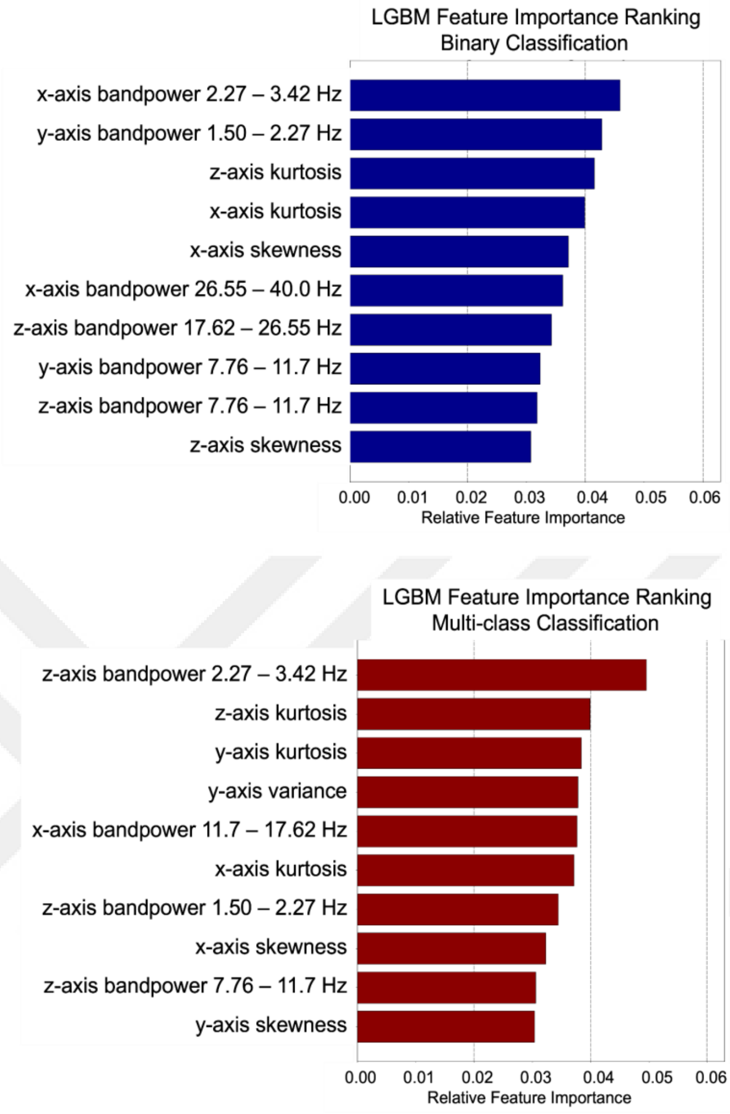

Figure 6: Feature Importance Ranking for the Binary and Multi-class Tasks

The feature importance results for both tasks are presented in Figure 6. Overall, bandpowers, kurtosis, and skewness were the most influential features in both the binary and multi-class classification tasks. Since kurtosis represents the tailedness and skewness represents asymmetry in the data, these features serve as important indicators of how the data is distributed. The prominence of kurtosis and skewness from multiple axes as the most important features suggests that the distributions of different breathing episodes varied significantly from one another.

3.4 Conclusion

In this study, a novel hierarchical framework was developed using a simulated data collection protocol to assess the potential of SCG signals for apnea detection and respiration pace evaluation. The framework begins with a binary Light Gradient-Boosting Machine (LGBM) model trained to identify breath-holding (apnea) episodes. If the prediction does not indicate a breath-holding state, the data is then passed into a multi-class LGBM model to classify the episodes as normal, slow, or fast breathing. Overall, the binary LGBM model achieved an accuracy of 0.99, with recall, precision, and f1-score values of 0.95, 0.87, and 0.91, respectively. For the multi-class task, all metrics were 0.96. Furthermore, various window lengths (1, 2, 3, 4, and 5 seconds) were tested, with the optimal window length determined to be 5 seconds.

The results indicate that SCG signals contain significant information about changes in breathing patterns, suggesting their potential use in wearable systems as an alternative to the PSG test. Future work will focus on validating these findings with larger datasets, including real data from patients with sleep apnea.

CHAPTER 4: COMPARATIVE EVALUATION OF DENOISING ALGORITHMS FOR ENHANCED SCG SIGNAL PROCESSING DURING EXERCISE

4.1 Problem Statement

One of the biggest challenges in analyzing physiological signals in uncontrolled environments is the morphological distortions caused by motion-related noise. For this reason, many studies usually rely solely on data recorded during stationary rest periods. Unfortunately, motion-related noise cannot be addressed with filters typically used to remove out-of-band noise. This problem becomes even more significant as sensor sensitivity increases, causing even small movements to affect the parameters extracted from the signal.

In the literature, methods such as empirical mode decomposition (EMD) [Javaid et al., 2016, Lin et al., 2021], wavelet transform [Skoric et al., 2024], and deep learning [Nikbakht et al., 2023] stand out in SCG denoising. Among these studies, Nikbakht et al. used artificial noise at two different SNR levels to simulate noise addition; Skoric et al. manually added walking noise collected in a separate experiment to clean signals; Lin et al. incorporated subway vibration noise into physiological signals collected from pigs; and Javaid et al. focused on the data collected during treadmill walking. On the other hand, there are also studies in various fields focused on noise removal in other types of vibration signals. One of the most extensive areas is the removal of external noise from rotating machinery vibrations [Zhou et al., 2023]. Similar to physiological signal analysis, methods in this field predominantly center around empirical mode decomposition (EMD) and its advanced variations such as ensemble EMD (EEMD), complementary EEMD (CEEMD), and variational mode decomposition (VMD), etc.

In this work, we focus on the accurate estimation of the heart rate from SCG signals during rest and exercise periods. To that end, our contributions are as follows:

- We first assess the performance of four different SCG-based heart rate estimation methods during resting and exercise phases: (i) directly implementing peak finding, (ii) enveloping and peak finding, (iii) applying Teager-Kaiser operator and peak finding, and (iv) applying Teager-Kaiser operator, enveloping and peak finding.

- We evaluate and compare the improvement in the SCG-based heart rate estimation results under seven different denoising algorithms: EMD, EEMD, CEEMD, VMD, Savitzky-Golay, moving average and wavelet denoising.

4.2 Methods

4.2.1 Custom Wearable Patch

In this work, the wearable data was collected using a custom wearable patch developed in our research laboratory. The patch was allowing for the collection of electrocardiogram (ECG), seismocardiogram (SCG), photoplethysmogram (PPG) and temperature signals. For SCG and PPG signal acquisition, a digital ADXL355 accelerometer and a digital MAX30102 sensor were utilized, respectively. ECG recording was performed using an AD8232 analog front-end integrated circuit, with Einthoven's triangle generated by three gel electrodes. Signals from these electrodes were conditioned by the AD8232. Skin temperature was measured using an LMT70A temperature sensor. The ECG and temperature signals were sampled at 10-bit resolution with sampling rates of 500 Hz and 25 Hz, respectively. An ATMEGA2560 microcontroller managed the system, and the collected data was stored on a SanDisk Ultra microSD card. File naming was handled by a DS3231 real-time clock (RTC). The system operated on a 400 mAh Lithium-Polymer battery, charged by an LTC4062 charger. Hardware interrupts were implemented to optimize power management. Detailed hardware and firmware specifications are provided in [Hayirlioglu and Semiz, 2024].

4.2.2 Experimental Setup and Dataset Information

The study was conducted under a protocol approved by the Koc University Institutional Review Board (2021.284.IRB2.054). Prior to data collection, all subjects provided their written consent. 20 subjects (8 females and 12 males) participated in the study (age: 23.8 ± 4.2 years, height: 172.6 ± 9.5 cm, weight: 70.9 ± 16.1 kg).

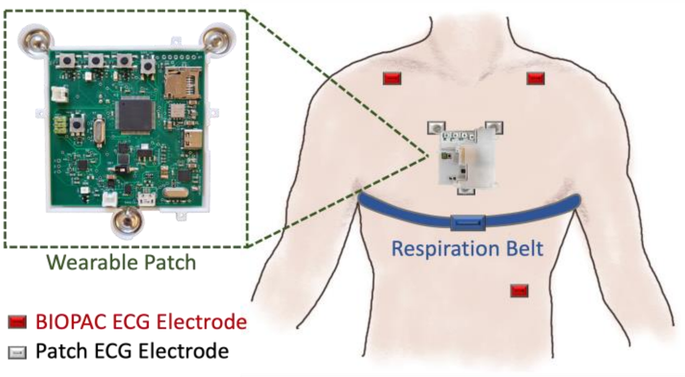

Figure 7: Sensors Locations

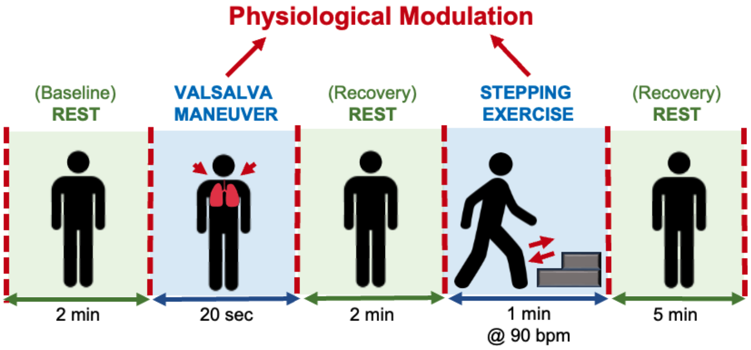

Figure 8: Experimental protocol

The wearable patch was affixed on the mid-sternum using three gel electrodes. Among the aforementioned patch signals, the SCG signal was primarily used in the analysis. On the other hand, the reference ECG and respiration signals were collected using the BIOPAC system. For ECG acquisition, an additional set of three gel electrodes was employed, and for respiration monitoring, a respiratory belt transducer was wrapped around the chest. The RSPEC-R module of the BIOPAC system wirelessly transmitted the signals from the electrodes and respiratory belt to the BIOPAC system. Detailed sensor attachments are illustrated in Figure 7.

The experimental protocol was designed to incorporate multiple steps, aiming to capture baseline signals during stationary conditions and monitor changes in response to physical modulations. In this study, the protocol included the Valsalva maneuver and stepping exercise as methods of physiological modulation, as illustrated in Figure 8. Participants began by standing still for 2 minutes, followed by a Valsalva maneuver. After a 2-minute

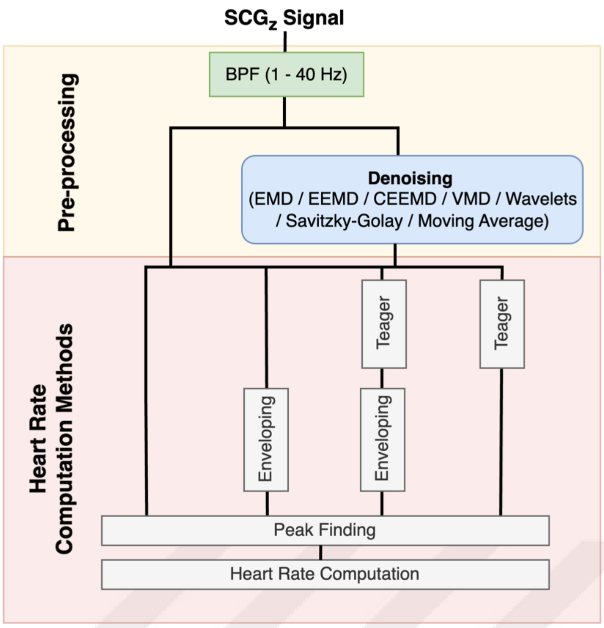

Figure 9: Study Pipeline

recovery period, the stepping exercise commenced, where participants stepped up and down at a rhythm of 90 bpm, guided by a metronome. The protocol concluded with a 5-minute recovery period.

4.2.3 Preprocessing

The signals were filtered using Kaiser window finite impulse response filter to remove out-of-band noise. Cut-off frequencies were determined as 1-40 and 0.5-40 for SCG and ECG, respectively. No additional preprocessing was needed for the ECG signals since they were already low-noise and suitable for peak detection. No additional preprocessing steps were applied to the SCG signals either, as this version of the signals were used for benchmarking against various filtered versions of themselves.

4.2.4 Heart Rate Computation in Resting Phase

For the resting heart rate computation, the region between the first 15-120 seconds (a total of 105 seconds) of the patch SCG and BIOPAC ECG was used. First, using the preprocessed ECG signal's peaks, baseline heart rate was calculated. The intervals between the consecutive R-peaks were computed to generate an RR difference vector. This vector was then used in Equation 5 to determine the heart rate (HR) in beats per minute (bpm), where *Fs* is the sampling frequency of the ECG signal.

$$HR = \frac{60 * Fs}{mean(RR)} \qquad (5)$$

SCG-based heart rate was then calculated using the SCG signal's z-axis, with four approaches: (i) directly implementing peak finding, (ii) enveloping and peak finding, (iii) applying Teager-Kaiser operator and peak finding, and (iv) applying Teager-Kaiser operator, enveloping and peak finding. These steps are visualized in Figure 9.

- *Peak finding:* Peak detection in SCG signals for heart rate calculation was done by identifying the successive maxima (i.e., aortic opening (AO) points), and measuring the time intervals between these peaks to determine the heart rate, similar to the ECG case.
- *Enveloping and peak finding:* Enveloping was done via Hilbert transforming the signal and taking the absolute value of it. Hilbert filter length was selected as 0.1 seconds. Following that the aforementioned peak detection algorithm was implemented.
- *Teager-Kaiser operator and peak finding:* Teager-Kaiser operator is a simple algorithm for calculating instantaneous energy of the signal [Kaiser, 1990]. We hypothesized that the AO points on the SCG signal could be more accurately identified using the Teager energy operator, even though they are not readily detectable with a simple peak detection algorithm. Hence, using Equation 6, we computed the Teager energy and leveraged the resulting peaks in the subsequent peak finding algorithm.
- *Teager-Kaiser operator, enveloping and peak finding:* A similar approach to the previous one has been leveraged, however the resulting Teager energy peaks were first enveloped, and then used in the subsequent peak finding algorithm.

$$\Phi_{TE}[n] = x[n]^2 - x[n+1]x[n-1] \qquad (6)$$

Following the heart rate computation using these three methods, the average percentage error and root mean squared error (RMSE) across 20 subjects with respect to the ECG reference was calculated using Equations 7 and 8, where n=20. The error observed during the resting phase was treated as the baseline error in SCG-based heart rate computation.

The objective during the subsequent exercise phase was thus to enhance the SCG-based heart rate calculation, aiming to approach this baseline error level.

4.2.5 Heart Rate Computation in Exercise Phase

For the exercise period, 45 seconds of the stepping exercise region was used both for the BIOPAC ECG and patch SCG signals. To compute the reference heart rate, the BIOPAC ECG was used. For the SCG-based computation, methods in the resting phase were used initially, without any extra filter. The error values with respect to the ECG reference were again calculated using Equations 7 and 8.

4.2.6 Denoising Algorithms

To lower the extra noise on the SCG signal during exercise and get better heart rate predictions, various filters and decomposition methods were applied on the SCG signals acquired during the exercise phase.

- *Empirical Mode Decomposition (EMD):* EMD applies decomposition of the signal into small number of intrinsic mode functions (IMF), which are suitable for Hilbert transform. This method is generally used with analyzing non-linear and non-stationary data [Huang et al., 1998]. Using this decomposition with the SCG signal, 6 IMFs were extracted for each individual. First IMF had the highest frequency, therefore it was used for peak detection.
- *Ensemble Empirical Mode Decomposition (EEMD):* It applies white noise to original signal ensembles, then calculates IMFs. These are later averaged in order to eliminate white noise and obtain the persistent part of the signal [Wu and Huang, 2009]. It is helpful for resolving mode-mixing problem that can happen in EMD because of noisy signal. In our task, standard deviation of white noise was selected as 0.05, and 5 ensembles were created. First IMF was used for peak detection.
- *Complementary Ensemble Empirical Mode Decomposition (CEEMD):* In order to get the persistent part in EEMD, many ensembles are needed to guarantee the average will remove the added white noise. Since this can be too time consuming, CEEMD uses complementaries of white noise (positive and negative), guaranteeing noise cancellation [Yeh et al., 2010]. In our task, standard deviation

of white noise was selected as 0.05, and 5 positive-negative ensemble pairs were created, and the first IMF was used for peak detection.

- *Variational Mode Decomposition (VMD):* It extracts the mode waveforms and central frequencies of the signal concurrently, unlike the EMD's sequential decomposition. It is known to be less sensitive to noise and signal sampling [Dragomiretskiy and Zosso, 2013]. The first IMF was used for peak detection.
- *Savitzky-Golay Denoising:* It uses convolution and linear least squares to fit subsets of the signal with a polynomial with arbitrary low-degree. It generates a smoothed (denoised) signal using the convolution coefficients [Savitzky and Golay, 1964]. In our task, polynomial degree was selected as 2 and subset frame length was selected 2/3 seconds.
- *Moving Average Denoising:* It is a particular case of Savitzky-Golay with a polynomial degree of 0. Each signal point becomes the average of the points of the subset. Subset frame length was selected 2/3 seconds.
- *Wavelet Decomposition:* Daubechies 6 wavelet was used as the mother wavelet, since its oscillation pattern is similar to the shape of heart beats. The signal was decomposed into 3 levels: 20-40 Hz, 10-20 Hz and 5-10 Hz. SCG signal was reconstructed using 5-10 and 10-20 Hz components, since the heart beat from SCG can contain the components above 7 Hz [Lin and Jhou, 2020].

In all cases, the resulting signals were used for peak detecting, by applying the methods presented in Section 4.2.4. The error values with respect to the ECG reference were again calculated using Equations 7 and 8.

$$MAPE = \frac{1}{n}\sum_{i=1}^{n}\left|\frac{ECG_{HR,i}-SCG_{HR,i}}{ECG_{HR,i}}\right| \qquad (7)$$

$$RMSE = \sqrt{\frac{\sum_{i=1}^{n}(ECG_{HR,i}-SCG_{HR,i})^2}{n}} \qquad (8)$$

Table 9: SCG Rest Data Heart Rate Calculation Performance

	MAPE	RMSE
Peak	0.053	6.337
Envelope + Peak	0.054	6.49
Teager + Peak	**0.052**	**6.281**
Teager + Envelope + Peak	0.060	7.015

4.3 Results and Discussion

4.3.1 Heart Rate Results for Rest and Exercise Phases

The results for the proposed heart rate computation algorithms are presented in Tables 9 and 10. For both rest and exercise phases, the combination of the Teager-Kaiser energy operator and peak detection algorithm resulted in the best performance (rest MAPE of 0.052 and exercise MAPE of 0.113). While the worst performing one in the resting state was the combination of Teager-Kaiser energy, enveloping and peak detection algorithm; the worst performing one in the exercise phase was implementing a direct peak detection algorithm, mainly because of the corruption in the maxima due to motion artifacts.

4.3.2 Effect of Enveloping

Enveloping the signal had a very small negative effect on the resting heart rate estimation. On the other hand, for exercising data, it provided a significant positive effect. Compared to the non-enveloped signals, enveloped signals showed 2% less MAPE on average, which corresponds to almost 17% relative improvement on MAPE. Best heart rate predicting from SCG pipeline was the one including enveloping steps.

Table 10: SCG Exercise Data Heart Rate Calculation Performance

WITHOUT DENOISING		
	MAPE	RMSE
Peak	0.145	19.354
Envelope + Peak	0.117	16.481
Teager + Peak	**0.113**	**16.296**
Teager + Envelope + Peak	0.126	17.566
WITH DENOISING		
	MAPE	RMSE
EMD + Peak	0.104	15.615
EMD + Envelope + Peak	0.097	15.065
EEMD + Peak	0.106	15.724
EEMD + Envelope + Peak	0.097	15.182
CEEMD + Peak	0.148	19.549
CEEMD + Envelope + Peak	0.150	19.456
VMD + Peak	0.110	16.095
VMD + Envelope + Peak	**0.090**	**13.936**
SG + Peak	0.198	28.519
SG + Envelope + Peak	**0.091**	**13.176**
MA + Peak	0.092	16.677
MA + Envelope + Peak	0.093	15.255
Wavelet + Peak	0.119	16.378
Wavelet + Envelope + Peak	0.103	15.138

4.3.3 Effect of Denoising Methods

Among the methods presented, EMD, EEMD and VMD decreased the MAPE. Specifically, when they were combined with enveloping, lowest errors were achieved (Table 10). Adding the Teager-Kaiser step resulted in worse performance compared to enveloping after denoising, hence those results were not presented for the sake of space. VMD with enveloping gave the best result, followed by Savitzky-Golay with enveloping. CEEMD itself did not decrease the MAPE, even with the addition of enveloping. Its total effect was positive but very small compared to other methods. Overall, compared to the case where no denoising was applied, MAPE reduced from 0.145 to 0.09; which indicates an absolute 5% and a relative 38% improvement in error.

4.4 Conclusion

In this work, a comparative analysis on different heart rate estimation and SCG denoising methods was presented. Overall, variational mode decomposition and Savitzky-Golay denoising resulted in the least MAPE and RMSE in SCG-based heart rate values during exercising. The results show that the dorsoventral SCG signal can be used as a good estimator for heart rate during mobile tasks, when analyzed with appropriate denoising algorithms. Future work will focus on validating the results in larger datasets including different modulation tasks and higher number of subjects.

CHAPTER 5: **CONCLUSION**

In conclusion, this thesis demonstrated significant advancements in the analysis and application of SCG signals, addressing challenges such as noise removal, event detection, and physiological parameter estimation. Through the development of novel algorithms and analysis frameworks, we showcased the potential of SCG signals for tasks like systolic time interval (LVET and PEP) estimation, heart rate calculation, apnea detection, and breathing pattern assessment. Additionally, our comparative evaluation of denoising methods, highlighted the importance of selecting optimal preprocessing techniques for improving signal quality.

In Chapters 2 and 3, the use of SCG signals for determining systolic time intervals and detecting apnea is explored. Both methods rely on straightforward tree-based algorithms for prediction and classification, combined with basic preprocessing and feature extraction techniques. As a result, these applications are well-suited for real-time implementation on wearable devices. However, a significant challenge arises from motion artifacts that can distort the SCG signal. To address this, Chapter 4 introduces real-time denoising methods designed to mitigate the impact of these artifacts.

Overall, the integration of SCG signals into wearable systems, combined with optimized processing techniques, offers a promising approach to enhancing traditional diagnostic methods. These findings collectively emphasize the versatility and potential of SCG in advancing personalized healthcare, particularly in wearable health monitoring and continuous physiological assessment.

Chapter 2 of this thesis is published with the title "Unveiling the Temporal and Spectral Relationships between Seismocardiogram Signals, Systolic Time Intervals and Thorax Characteristics” [Kizir and Semiz, 2023].

Chapter 3 of this thesis is published with the title “A Hierarchical Framework for Apnea Detection and Respiration Pace Assessment Using Seismocardiogram Signals” [Kizir and Semiz, 2024].

BIBLIOGRAPHY

[Altevogt and Cohen, 2006] Altevogt, B. M., & Colten, H. R. (Eds.). (2006). Sleep disorders and sleep deprivation: an unmet public health problem.

[Breiman, 2001] Breiman, L. (2001). Random forests. Machine learning, 45:5–32.

[Chen and Guestrin, 2016] Chen, T., & Guestrin, C. (2016, August). Xgboost: A scalable tree boosting system. In *Proceedings of the 22nd acm sigkdd international conference on knowledge discovery and data mining* (pp. 785-794).

[Cheol Jeong et al., 2018] Cheol Jeong, I., Bychkov, D., & Searson, P. C. (2018). Wearable devices for precision medicine and health state monitoring. *IEEE Transactions on Biomedical Engineering*, *66*(5), 1242-1258.

[Di Rienzo et al., 2013] Di Rienzo, M., Vaini, E., Castiglioni, P., Meriggi, P., & Rizzo, F. (2013, July). Beat-to-beat estimation of LVET and QS2 indices of cardiac mechanics from wearable seismocardiography in ambulant subjects. In *2013 35th Annual International Conference of the IEEE Engineering in Medicine and Biology Society (EMBC)* (pp. 7017-7020). IEEE.

[Dragomiretskiy and Zosso, 2013] Dragomiretskiy, K., & Zosso, D. (2013). Variational mode decomposition. *IEEE transactions on signal processing*, *62*(3), 531-544.

[Erin and Semiz, 2023] Erin, E., & Semiz, B. (2023). Spectral Analysis of Cardiogenic Vibrations to Distinguish Between Valvular Heart Diseases. In *BIOSIGNALS* (pp. 212-219).

[Imirzalioglu and Semiz, 2022] Imirzalioglu, M., & Semiz, B. (2022, July). Quantifying respiration effects on cardiac vibrations using teager energy operator and gradient boosted trees. In *2022 44th Annual International Conference of the IEEE Engineering in Medicine & Biology Society (EMBC)* (pp. 1935-1938). IEEE.

[Hayirlioglu and Semiz, 2023] Hayirlioglu, Y. Z., & Semiz, B. (2023). A Novel Multi-Modal Sensing System Prototype for Cardiovascular and Cardiopulmonary Monitoring. In *BIODEVICES* (pp. 126-134).

[Hayirlioglu and Semiz, 2024] Hayirlioglu, Y. Z., & Semiz, B. (2024). PhysioPatch: A Multi-modal and Adaptable Wearable Patch for Cardiovascular and Cardiopulmonary Assessment. *IEEE Sensors Journal*.

[Huang et al., 1998] Huang, N. E., Shen, Z., Long, S. R., Wu, M. C., Shih, H. H., Zheng, Q., ... & Liu, H. H. (1998). The empirical mode decomposition and the Hilbert spectrum for nonlinear and non-stationary time series analysis. *Proceedings of the Royal Society of London. Series A: mathematical, physical and engineering sciences*, *454*(1971), 903-995.

[Hurnanen et al., 2016] Hurnanen, T., Lehtonen, E., Tadi, M. J., Kuusela, T., Kiviniemi, T., Saraste, A., ... & Pänkäälä, M. (2016). Automated detection of atrial fibrillation based on time–frequency analysis of seismocardiograms. *IEEE journal of biomedical and health informatics*, *21*(5), 1233-1241.

[Inan et al., 2018] Inan, O. T., Baran Pouyan, M., Javaid, A. Q., Dowling, S., Etemadi, M., Dorier, A., ... & Klein, L. (2018). Novel wearable seismocardiography and machine learning algorithms can assess clinical status of heart failure patients. *Circulation: Heart Failure*, *11*(1), e004313.

[Inan et al, 2014] Inan, O. T., Migeotte, P. F., Park, K. S., Etemadi, M., Tavakolian, K., Casanella, R., ... & Di Rienzo, M. (2014). Ballistocardiography and seismocardiography: A review of recent advances. *IEEE journal of biomedical and health informatics*, *19*(4), 1414-1427.

[Javaid et al., 2015] Javaid, A. Q., Fesmire, N. F., Weitnauer, M. A., & Inan, O. T. (2015, June). Towards robust estimation of systolic time intervals using head-to-foot and dorso-ventral components of sternal acceleration signals. In *2015 IEEE 12th international conference on wearable and implantable body sensor networks (BSN)* (pp. 1-5). IEEE.

[Javaid et al., 2016] Javaid, A. Q., Ashouri, H., Dorier, A., Etemadi, M., Heller, J. A., Roy, S., & Inan, O. T. (2016). Quantifying and reducing motion artifacts in wearable seismocardiogram measurements during walking to assess left ventricular health. *IEEE Transactions on Biomedical Engineering*, *64*(6), 1277-1286.

[Kaiser, 1990] Kaiser, J. F. (1990, April). On a simple algorithm to calculate the'energy'of a signal. In *International conference on acoustics, speech, and signal processing* (pp. 381-384). IEEE.

[Ke at al., 2017] Ke, G., Meng, Q., Finley, T., Wang, T., Chen, W., Ma, W., ... & Liu, T. Y. (2017). Lightgbm: A highly efficient gradient boosting decision tree. *Advances in neural information processing systems*, *30*.

[Kizir and Semiz, 2023] Kizir, B., & Semiz, B. (2023, June). Unveiling the Temporal and Spectral Relationships between Seismocardiogram Signals, Systolic Time Intervals and Thorax Characteristics. In *2023 5th International Conference on Bio-engineering for Smart Technologies (BioSMART)* (pp. 1-4). IEEE.

[Kizir and Semiz, 2024] Kizir, B., & Semiz, B. (2024). A Hierarchical Framework for Apnea Detection and Respiration Pace Assessment Using Seismocardiogram Signals. In *BIOSTEC (1)* (pp. 793-798).

[Klum et al., 2020] Klum, M., Urban, M., Tigges, T., Pielmus, A. G., Feldheiser, A., Schmitt, T., & Orglmeister, R. (2020). Wearable cardiorespiratory monitoring employing a multimodal digital patch stethoscope: estimation of ECG, PEP, LVET and respiration using a 55 mm single-lead ECG and phonocardiogram. *Sensors*, *20*(7), 2033.

[Kwon et al., 2021] Kwon, S., Kim, H., and Yeo, W.-H. (2021). Recent advances in wearable sensors and portable electronics for sleep monitoring. Iscience, 24(5)

[Lewis et al., 1977] Lewis, R. P., Rittogers, S. E., Froester, W. F., & Boudoulas, H. (1977). A critical review of the systolic time intervals. *Circulation*, *56*(2), 146-158.

[Lin and Jhou, 2020] Lin, Y. D., & Jhou, Y. F. (2020). Estimation of heart rate and respiratory rate from the seismocardiogram under resting state. *Biomedical Signal Processing and Control*, *57*, 101779.

[Lin et al., 2021] Lin, D. J., Kimball, J. P., Zia, J., Ganti, V. G., & Inan, O. T. (2021). Reducing the impact of external vibrations on fiducial point detection in seismocardiogram signals. *IEEE Transactions on Biomedical Engineering*, *69*(1), 176-185.

[Nikbakht et al., 2023] Nikbakht, M., Lin, D. J., & Inan, O. T. (2023, October). Learning Seismocardiogram Beat Denoising Without Clean Data. In *2023 IEEE EMBS International Conference on Biomedical and Health Informatics (BHI)* (pp. 1-4). IEEE.

[Odinaka et al., 2012] Odinaka, I., Lai, P. H., Kaplan, A. D., O'Sullivan, J. A., Sirevaag, E. J., & Rohrbaugh, J. W. (2012). ECG biometric recognition: A comparative analysis. *IEEE Transactions on Information Forensics and Security*, *7*(6), 1812-1824.

[Padilla-Ortiz and Ibarra, 2018] Padilla-Ortiz, A. L., & Ibarra, D. (2018). Lung and heart sounds analysis: state-of-the-art and future trends. *Critical Reviews™ in Biomedical Engineering*, *46*(1).

[Pandia et al., 2012] Pandia, K., Inan, O. T., Kovacs, G. T., & Giovangrandi, L. (2012). Extracting respiratory information from seismocardiogram signals acquired on the chest using a miniature accelerometer. *Physiological measurement*, *33*(10), 1643.

[Philips 2019] Philips (2019). The global pursuit of better sleep health.

[Salerno et al., 1992] Salerno, D. M., Zanetti, J. M., Poliac, L. C., Crow, R. S., Hannan, P. J., Wang, K., ... & Van Tassel, R. A. (1992). Exercise seismocardiography for detection of coronary artery disease. *American journal of noninvasive cardiology*, *6*(5), 321-330.

[Sana et al., 2020] Sana, F., Isselbacher, E. M., Singh, J. P., Heist, E. K., Pathik, B., & Armoundas, A. A. (2020). Wearable devices for ambulatory cardiac monitoring: JACC state-of-the-art review. *Journal of the American College of Cardiology*, *75*(13), 1582-1592.

[Savitzky and Golay, 1964] Savitzky, A., & Golay, M. J. (1964). Smoothing and differentiation of data by simplified least squares procedures. *Analytical chemistry*, *36*(8), 1627-1639.

[Semiz et al., 2020] Semiz, B., Carek, A. M., Johnson, J. C., Ahmad, S., Heller, J. A., Vicente, F. G., ... & Inan, O. T. (2020). Non-invasive wearable patch utilizing seismocardiography for peri-operative use in surgical patients. *IEEE journal of biomedical and health informatics*, *25*(5), 1572-1582.

[Shandhi et al., 2019] Shandhi, M. M. H., Semiz, B., Hersek, S., Goller, N., Ayazi, F., & Inan, O. T. (2019). Performance analysis of gyroscope and accelerometer sensors for seismocardiography-based wearable pre-ejection period estimation. *IEEE journal of biomedical and health informatics*, *23*(6), 2365-2374.

[Sherwood et al., 1990] Sherwood, A., Allen, M. T., Fahrenberg, J., Kelsey, R. M., Lovallo, W. R., & Van Doornen, L. J. (1990). Methodological guidelines for impedance cardiography. *Psychophysiology*, *27*(1), 1-23.

[Skoric et al., 2024] Skoric, J., D'Mello, Y., & Plant, D. V. (2024). A Wavelet-Based Approach for Motion Artifact Reduction in Ambulatory Seismocardiography. *IEEE Journal of Translational Engineering in Health and Medicine*.

[Song and Ying, 2015] Song, Y.-Y. and Ying, L. (2015). Decision tree methods: applications for classification and prediction. Shanghai archives of psychiatry, 27(2):130.

[Summers et al., 2003] Summers, R. L., Shoemaker, W. C., Peacock, W. F., Ander, D. S., & Coleman, T. G. (2003). Bench to bedside: electrophysiologic and clinical principles of noninvasive hemodynamic monitoring using impedance cardiography. *Academic emergency medicine*, *10*(6), 669-680.

[Tavakolian, 2016] Tavakolian, K. (2016). Systolic time intervals and new measurement methods. *Cardiovascular engineering and technology*, *7*, 118-125.

[Wilson et al., 1993]. Wilson, R. A., Bamrah, V. S., Lindsay Jr, J., Schwaiger, M., & Morganroth, J. (1993). Diagnostic accuracy of seismocardiography compared with electrocardiography for the anatomic and physiologic diagnosis of coronary artery disease during exercise testing. *The American journal of cardiology*, *71*(7), 536-545.

[Wu and Huang, 2009] Wu, Z., & Huang, N. E. (2009). Ensemble empirical mode decomposition: a noise-assisted data analysis method. *Advances in adaptive data analysis*, *1*(01), 1-41.

[Xu et al., 2014] Xu, Q., Nwe, T. L., & Guan, C. (2014). Cluster-based analysis for personalized stress evaluation using physiological signals. *IEEE journal of biomedical and health informatics*, *19*(1), 275-281.

[Yang et al., 2020] Yang, C., Aranoff, N. D., Green, P., & Tavassolian, N. (2019). Classification of aortic stenosis using time–frequency features from chest cardio-mechanical signals. *IEEE Transactions on Biomedical Engineering*, *67*(6), 1672-1683.

[Yeh et al., 2010] Yeh, J. R., Shieh, J. S., & Huang, N. E. (2010). Complementary ensemble empirical mode decomposition: A novel noise enhanced data analysis method. *Advances in adaptive data analysis*, *2*(02), 135-156

[Zhou et al., 2023] Zhou, X., Wang, X., Wang, H., Xing, Z., Yang, Z., & Cao, L. (2023). Method for denoising the vibration signal of rotating machinery through VMD and MODWPT. *Sensors*, *23*(15), 6904.